

Acquisition-free Nyquist ghost correction for parallel imaging accelerated EPI

Eric Peterson¹, Murat Aksoy¹, Julian Maclaren¹, and Roland Bammer¹

¹Department of Radiology, Stanford University, Stanford, California, United States

Target Audience: Researchers interested in parallel imaging accelerated echo planar imaging (EPI), especially those using prospective motion correction or long scans, where conventional ghost correction performs poorly.

Purpose: Echo planar imaging is commonly used in many applications including diffusion and perfusion imaging, which often employ techniques such as motion correction, dynamic imaging, and simultaneous multi-slice (SMS) imaging. In each of these cases, Nyquist ghost correction is required to correct for inconsistencies between the left and right sampled k-space lines. Previous works have shown that single shot imaging can be effectively de-ghosted using the image entropy^{1,2}. However, entropy cannot reliably de-ghost individual shots in a multi-shot or SMS blipped-CAIPIRINHA³ acquisition, because entropy-based ghost correction minimizes the ghosting artifacts in the image, which are confounded by the aliasing in these cases. Another case in which shot-by-shot ghost-correction is vital is prospectively motion corrected single or multi-shot EPI data because the ghost-correction parameters change as the subject and FOV moves. **Therefore, this work demonstrates a method for Nyquist ghost correction, based on singular value decomposition (SVD), which works on individual shots of parallel imaging acquisitions.**

Theory: The deghosting method proposed here is similar to the image entropy minimization technique proposed by Nordell et al¹; however, rather than minimizing image entropy, the proposed technique seeks to maximize the self-consistency of neighboring k-space points (before ramp sampling correction) by shifting and phasing the left and right sampled k-space lines. Because consistency can be difficult to define, the data are grouped into GRAPPA-like kernels (Fig. 1, top left), and each kernel becomes a column in a matrix M (Fig. 1, top right) with dimensions r -by- c , where r is the total number of k-space points in the kernel for all receive coils ($n_{x_{kernel}} \times n_{y_{kernel}} \times n_{coils}$) and c is the total number of kernels, typically covering the whole k-space. The SVD decomposition of $M=U\Sigma V^H$, where the diagonal of Σ represents the singular values, is shown in Fig. 2 and the bottom right of Fig. 1 and is the basis for the minimization. The singular values are a surrogate for data consistency, with more consistent data having much more energy in the initial singular values and inconsistent data having the energy more evenly distributed across the singular values. In order to promote data consistency, the sum of the tail of the singular values from n to the end, N , (where n is defined based on the estimated rank of the matrix) is minimized using unconstrained optimization which seeks to correctly align the left and right sampled k-space lines by shifting and phasing (Fig. 1 bottom left). Note that the SVD methodology is similar to what is used by Shin et al⁴ in their calibrationless parallel imaging reconstruction.

Methods: Acquisitions: Two schemes were evaluated: 1. **Dynamic EPI with optical prospective motion correction.** A pulse sequence with real-time motion correction using an optical motion tracking setup⁵ was used to scan a volunteer who moved during the scan using an 8-channel head coil (Invivo, Best, The Netherlands). 2. **SMS EPI.** An SMS-enabled blipped-CAIPIRINHA pulse sequence was used to scan a volunteer with two simultaneous slices using a 32-ch head coil (Nova Medical, Wilmington, MA, USA). All images were acquired on a GE 3T scanner (MR750, GE Healthcare, Waukesha, WI, USA). **Reconstruction:** All images were acquired fully sampled, which allowed for standard single shot reconstruction using the FFT. To demonstrate the capability of the SVD-based optimization, the images were undersampled for the ghost correction step alone – effectively simulating parallel imaging – and the final reconstruction used the complete image data. For the prospective motion-corrected dynamic EPI acquisition, entropy-based ghost correction was also performed for comparison.

Results and Discussion: Figure 2 shows how, through reduction of the singular values after n , the Nyquist ghosting can be removed and indicates how the data consistency is reflected in the singular values. Figure 3 shows Nyquist ghost correction used in conjunction with prospective motion correction. Note how - without correction at each frame - the Nyquist ghosting can be significant when motion occurs (A-C). Also note that entropy ghost correction does not work reliably when using parallel imaging acceleration without a calibration scan (D-F), whereas the SVD-based optimization works well (G-I), although some motion-induced ghosting remains. Figure 4 demonstrates that the SVD-based optimization also works well for SMS data, even with CAIPIRINHA blips and in-plane acceleration. It is worth noting, however, that the calculation of the SVD-based correction takes about 10 times longer than the entropy-based correction, however this can be reduced by performing coil compression or k-space cropping before computation. Moreover, it should be noted that no conversion into the image domain is needed in each iteration, as compared to the image-based entropy method.

Conclusion: The method described here allows for a reduction of scan time (i.e., no need for a reference scan) as well as the possibility for retrospective Nyquist ghost correction on individual shots. This provides robust, simple, and reliable EPI ghost correction even in cases with parallel and SMS imaging. Furthermore, this method can be applied in cases where a standard calibration may be insufficient or changes during a scan, such as when the gradients are rotated during prospective motion correction.

References: 1) Nordell A et al, ISMRM 2007:1833. 2) Peterson et al, ISMRM 2014:1637. 3) Setsompop et al, MRM 2012; 67, 1210-24. 4) Shin et al, MRM 2014, 72:959-70. 5) Aksoy et al, MRM 2011, 66, 366-78.

Acknowledgements: NIH (5R01EB011654, 5R01EB008706, 5R01EB002711, P41 RR009784, P41 EB015891), Lucas Foundation.

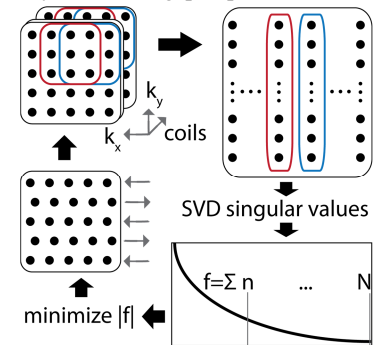


Figure 1: A flowchart of the SVD optimization algorithm, which minimizes the sum of the singular values from n to N to find the optimal phase and k-space shifts to minimize ghosting.

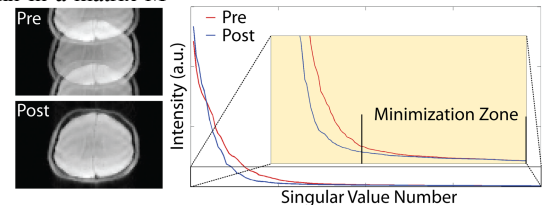


Figure 2: Pre and post ghost correction images and their respective SVD energy curves are shown. This demonstrates that minimizing the tail of the curve is a reliable metric to use to correct Nyquist ghosting.

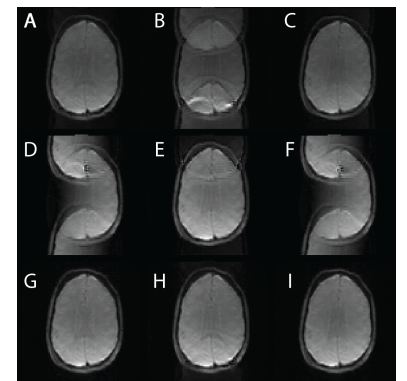


Figure 3: Columns show temporal timepoints of motion corrected images with head rotations of 3° (A,D,G), 8° (B,E,H), and 1° (C,F,I). A-C) Constant Nyquist ghost correction set from the first frame. D-F) Entropy-based Nyquist ghost correction using a parallel imaging acceleration of 3. G-I) SVD-based Nyquist ghost correction using a parallel imaging acceleration of 3.

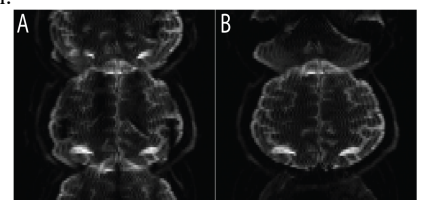


Figure 4: Pre and post SVD-based Nyquist ghost correction images using a blipped-CAIPIRINHA SMS scan with in-plane and slice accelerations of 3 and 2 respectively.